JOURNAL OF COMPUTATIONAL PHYSICS 112, 394–403 (1994)

Application of Fifth-Order Compact Upwind Differencing to Moisture Transport Equation in Atmosphere

MIKHAIL A. TOLSTYKH

Institute of Numerical Mathematics, Russian Academy of Sciences, Leninskii prosp. 32A, 117334 Moscow, Russia

Received August 10, 1992; revised December 28, 1993

This paper has two aims. The first aim is to investigate the behavior of recently introduced fifth-order compact upwind differencing (CUD-5) in conjunction with different high-order time stepping schemes by the examples of 1D and 2D advection (including the test on the sphere with the flow over the poles). The second aim is to demonstrate the power of CUD-5 with moisture transport equation in general circulation model of the atmosphere.

The problem of moisture transport in general circulation model of the atmosphere (GCMA) incorporates very steep, rapidly changing gradients. Besides, the moisture is essentially positive function and erroneous negative values can cause problems of a physical or numerical nature in GCMA. Moisture transport places rigid constraints on the numerical algorithm. These demands were discussed in [1]. Here we note that in this problem the main goal of the algorithm design is to provide conservation and quasi-monotonicity (i.e., the absence of spurious oscillations) properties simultaneously as well as the absence of negative values. It is well known that in some modern high-accuracy schemes the absence of spurious oscillations is provided by introducing an artificial dissipation in the vicinity of steep gradients of solution (FCT, TVD). However, if you are to simulate the impact of CO_2 or ozone on the atmosphere you should integrate GCMA for a very long time and artificial dissipation may result in unrealistically smooth distributions. Many works were devoted to this problem (see, for example, [1–3]). The aim of this work is to produce an efficient algorithm in Eulerian formulation for solving a moisture transport equation on the basis of the recently developed fifth-order compact upwind differencing and high-order implicit time-stepping meeting the above-mentioned demands.

1. FIFTH-ORDER COMPACT UPWIND DIFFERENCING

The fifth-order compact upwind differencing (CUD-5) was introduced in 1991 [4]. It has remarkable properties of small phase errors and dissipation concentrated on short waves. Complete derivation of CUD-5 is presented in [4]. Here we describe the idea of its construction.

On a difference grid with constant step h we construct the fifth-order accurate operator of the first differentiation using the first-order upwind operator $\Lambda(s)$ of the form

$$\begin{aligned} \Lambda(s)\, f &= (\Lambda_0 - s\,\Lambda_2)\, f, \\ \Lambda_0 f &= f_{i+1} - f_{i-1}, \\ \Lambda_2 f &= f_{i+1} - 2f_i + f_{i-1}. \end{aligned} \tag{1}$$

For the operator of first differentiation $D_x = \partial/\partial x$ we write formal series

$$D_x = \frac{1}{2h}\Lambda(s) + \left(I - \frac{1}{3s} h\, D_x + \frac{1}{12} h^2 D_x^2 - \frac{1}{60s} h^3 D_x^3\right) \times \frac{s}{2} h\, D_x^2, \tag{2}$$

where non-zero parameter s is supposed to be constant. We replace the expression in parentheses by the operator Padé approximant $P^{[m/n]} = R^{-1}Q$ [5] with accuracy $O(h^{m+n+1})$, where

$$\begin{aligned} R &= I + \sum_{k=1}^{n} b_k^{m,n} (h\, D_x)^k, \\ Q &= I + \sum_{k=1}^{m} a_k^{m,n} (h\, D_x)^k, \end{aligned} \tag{3}$$

and I is the identity operator. To ensure total fifth-order accuracy we use the approximants $P^{[2/1]}$ and $P^{[1/2]}$.

Further, we construct difference operators Q_h and R_h satisfying the following two conditions:

(i) The operator $R_h^{-1}Q_h$ approximates $R^{-1}Q$ with the error $O(h^4)$.

(ii) The number of nodes of the scheme for R_h may not exceed three.

0021-9991/94 $6.00

For this construction we utilize formulas of third order [10]:

$$D_x = \frac{1}{2h}(A(s_1))^{-1}\Delta(s_1) + O(h^3),$$

$$A(s_1) = I + \frac{\Delta_2}{6} - \frac{s_1}{4}\Delta_0, \tag{4}$$

$$s_1 = \text{const} \neq 0.$$

If we apply them to the operator Q_h, then conditions (i) and (ii) result in the operators R_h and Q_h:

$$R^{(1)} = I + \frac{1}{6s}\Delta_0 + \frac{1}{5}\Delta_2,$$
$$Q^{(1)} = I + \left(\frac{17}{60} - \frac{1}{9s^2}\right)\Delta_2. \tag{5}$$

Applying the operators (4) to both operators R_h and Q_h and taking into account conditions (i)–(ii), we obtain that for $|s| = 2/\sqrt{5}$ these operators become

$$R^{(2)} = I + \left(\frac{b}{2} - \frac{s_1}{4}\right)\Delta_0 + \left(\frac{1}{6} - \frac{b}{2}s_1\right)\Delta_2,$$
$$Q^{(2)} = I + \left(\frac{a}{2} - \frac{s_1}{4}\right)\Delta_0 + \left(\frac{1}{6} - \frac{a}{2}s_1\right)\Delta_2, \tag{6}$$
$$a = -\frac{2}{15s}, \qquad b = \frac{1}{5s}.$$

Using now the Padé operator approximant $D_x^2 = (I + \Delta_2/12)^{-1}\Delta_2/h^2 + O(h^4)$, we construct the operator

$$L_h(u) = \frac{1}{2h}\left(\Delta(s) + sR_h^{-1}Q_h\left(I + \frac{1}{12}\Delta_2\right)^{-1}\Delta_2\right)u. \tag{7}$$

Depending on the type of discretization for R_h and Q_h we will denote the corresponding operator L_h as $L_5^{(1)}$ or $L_5^{(2)}$. Parameters s and s_1 should change their sign as usual in upwind schemes.

One can see that this approximation of spatial derivative requires inversion of tridiagonal operators. It was proved in [4] that operators (5) and (6) are positive definite for $s > 0$ or negative definite for $s < 0$ if $|s| > \sqrt{5/3}$ in the case of operators (5) and $\operatorname{sgn} s_1 = \operatorname{sgn} s$, $|s_1| > \frac{5}{24}$ in the case of operators (6). The proper choice of s (upwinding) provides the stability of CUD-5 for frozen coefficients approximaton. Dispersion and dissipation properties of these operators are described in the Appendix. Here we note that the parameters s_1 of $L_5^{(2)}$, as well as s for $L_5^{(1)}$, controls phase error and dissipation for waves in the range of $2h$ to $6h$: the greater s_1 (or respectively s), the greater is the dissipation. The choice of these parameters has also to a certain extent an effect on the stability limit (see the Appendix). The cost of this discretization is at least 21 arithmetic operations per grid point.

In the grid points where velocity changes its sign, the direct application of such spatial discretization leads to the loss of the conservation property. To preserve this property, the idea of flux splitting suggested in the early eighties can be used [8, 9]. The flux splitting leads to an increase of the amount of arithmetic operations, but now both three-point operators R_h and $I + \Delta_2/12$ can be inverted in advance.

For the first type of CUD-5 several 1D tests suggested by Carpenter *et al.* [3] and 2D advection test were performed [7]. In these tests several types of implicit time stepping were checked with a focus on third-order schemes. The reasons for such a choice are as follows.

The limitation of CFL ≈ 1 imposed on the time step for moisture transport in Eulerian formulation is quite natural due to the approximation requirements. Therefore we need only to provide conditional stability. Routine explicit time stepping is usually used with CFL numbers which are small enough to provide sufficient stability and a small error due to time stepping. Thus computational efficiency of CUD-5 may become quite sufficient, if the computations are performed with CFL numbers ≈ 1 and the errors due to time stepping are negligible. So the reason for selecting time stepping of sufficiently high order in this paper is its accuracy for all admissible CFL numbers.

In tests for a 1D advection equation written in conservative form,

$$\frac{\partial q}{\partial t} + \frac{\partial uq}{\partial x} = 0, \tag{8}$$

several implicit time schemes were tested [7]. Here we use the best of these schemes—Adams third-order implicit scheme,

$$q^{n+1} - q^n = -\tau\left(\tfrac{5}{12}L_h(uq^{n+1}) + \tfrac{8}{12}L_h(uq^n) - \tfrac{1}{12}L_h(uq^{n-1})\right), \tag{9}$$

and the explicit Runge–Kutta third-order method,

$$q^{(1)} = L_h(u^n q^n),$$
$$q^{(2)} = L_h\left(u^{n+1/3}\left(q^n - \frac{\tau}{3}q^{(1)}\right)\right),$$
$$q^{(3)} = L_h\left(u^{n+2/3}\left(q^n - \frac{2\tau}{3}q^{(2)}\right)\right), \tag{10}$$
$$q^{n+1} - q^n = -\frac{\tau}{4}(q^{(1)} + 3q^{(3)}).$$

Optimum time stepping should provide minimum errors for the whole range of admissible CFL numbers. So tests should be performed for different CFL numbers, taking into account that for small CFL numbers all time integration schemes usually provide negligible errors. As will be clear from the further discussion, a certain disadvantage of the paper [7] was that all tests were performed only for CFL = 0.5, as well as those in the paper of Carpenter *et al.* [3].

Now we consider 1D tests suggested in [3] for the spatial discretization $L_5^{(2)}$ in conjunction with the two third-order time stepping schemes (9) and (10). These tests are described by Eq. (8) in the periodic interval of 40 points for rectangle and triangle distributions or 80 grid points for a Gaussian initial distribution with constant velocity. One hundred time steps were performed for rectangle and triangle distributions, while for the Gaussian distribution, 800 time steps were performed. Implicit time stepping was implemented using a GMRES solver with a Hausholder transformation [11]. The results of these tests for time stepping (9) and (10) and CFL = 0.5 are shown on Figs. 1A and B, respectively. The better results for the rectangle initial distribution were obtained when flux corrected transport (FCT) [13] was applied to the solution at each 10th time step (not shown). Comparing these curves with those for $L_5^{(1)}$ (Fig. 2) one can obviously see that $L_5^{(2)}$ provides better results. Increasing the parameter s for $L_5^{(1)}$ one can achieve the same extreme values of the distribution as for $L_5^{(2)}$ tests but the phase error becomes noticeable in this case (not shown).

The comparison of many other schemes (among them van Leer and Smolarkiewicz schemes) was given in [3]; the best results in this paper being for the piecewise parabolic method (PPM). We may note that CUD-5 in the case of a Gaussian initial distribution gives a better curve than PPM [3], where the maximum decreases to 0.881. For the triangle distribution they are comparable: PPM decreases the maximum to 0.768 without a steepening procedure and to 0.828 with steepening, the shape of the distribution in the latter case being similar to the rectangle. PPM generates no spurious negative values. In the case of $L_5^{(2)}$ we have the maximum value 0.868 with the maximum negative value −0.017. Applying FCT periodically one can eliminate the negative value in this test, the maximum value being about 0.75 (not shown). The results of applying $L_5^{(2)}$ for the rectangle distribution are worse than that of PPM since $L_5^{(2)}$ cannot simulate the waves with lengths $2h$ and $3h$ properly. It is also worth mentioning that the PPM is more expensive than CUD-5. As for time stepping, the schemes (9) and (10) provide comparable results for CFL = 0.5, as was in the case of $L_5^{(1)}$ [7].

Let us discuss the role of the parameter s_1 in $L_5^{(2)}$. As is shown in the Appendix, the optimum choice from the viewpoint of phase error is $s_1 = 1.1$, but when increasing s_1 the stability limit of time stepping (9) also increases. All the results for 1D tests with time stepping (9) were obtained at $s_1 = 2.05$. If one sets greater s_1, the results will be smoother

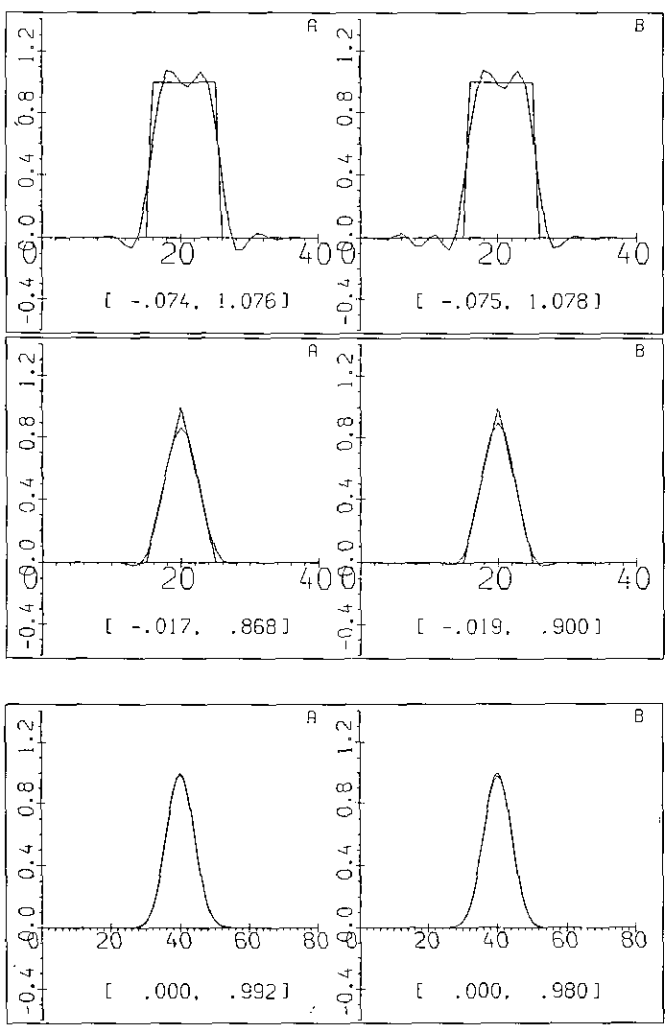

FIG. 1. 1D advection with $L_5^{(2)}$ in the periodical interval for different types of initial distribution, CFL = 0.5: A—time stepping (9), B—time stepping (10).

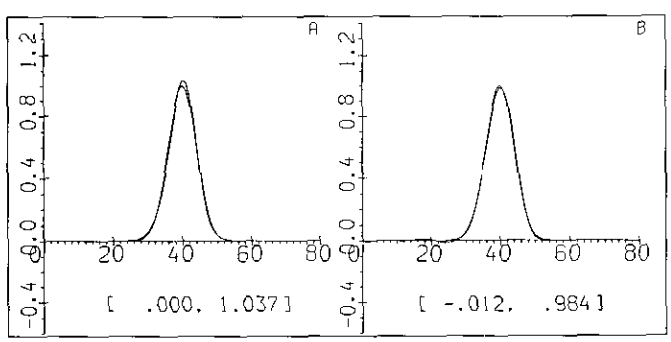

FIG. 2. 1D advection of Gaussian initial distribution with $L_5^{(1)}$, CFL = 0.5: A—time stepping (9), B—time stepping (10).

with much smaller undershoots, but the rectangle distribution in this case will be degenerated to a smooth wave (not shown). However, if we set $s_1 = 1.1$, a conditionally stable time scheme (9) demonstrates a very weak instability for the test with a Gaussian initial distribution and 800 time steps (the increase of the L_2 norm is about 2%—not shown). So if one uses unconditionally stable time stepping, the s_1 should be equal to 1.1 and the value $s_1 \approx 2$ may be recommended for time stepping (9). The same reasoning can be applied to $L_5^{(1)}$. The value of s corresponding to the minimal phase error is equal to 1.3 in this case and the recommended value for time stepping (9) is about 1.6. However, is was found during 2D tests for $L_5^{(2)}$ that the best results were obtained for $s_1 = 0.3$ which can be explained by the impact of boundary conditions. The same conclusion was drawn for Runge–Kutta time stepping. Hence, the choice of free parameters in $L_5^{(i)}$ in the case of conditionally stable time stepping seems to be dependent on the time integration scheme as well as on a given problem.

To verify these results and also to select the best time stepping, the 1D test for $L_5^{(2)}$ with Gaussian initial distribution was repeated for CFL = 0.875, $s_1 = 2.05$. In this case we are beyond the stability limit for time scheme (9) (see the Appendix) but due to the small enough amplifying factor we were able to obtain realistic solution after 800 time steps. The results are shown in Fig. 3. We may conclude that the Runge–Kutta method (10) provides better results due to its greater stability limit.

To investigate the shape-preserving property of the L_5 operators, a 2D advection test on the sphere with the flow directly over the poles was also carried out. This is the first test from the set of tests for shallow water equations in spherical geometry [12]. This test is important since near the poles meridians of the spherical coordinate system converge, resulting in local CFL numbers of order 10 near the poles. The test is described by the equation

$$\frac{\partial q}{\partial t} + \frac{1}{a \cos \varphi}\left(\frac{\partial uq}{\partial \lambda} + \frac{\partial v \cos \varphi q}{\partial \varphi}\right) = 0,$$

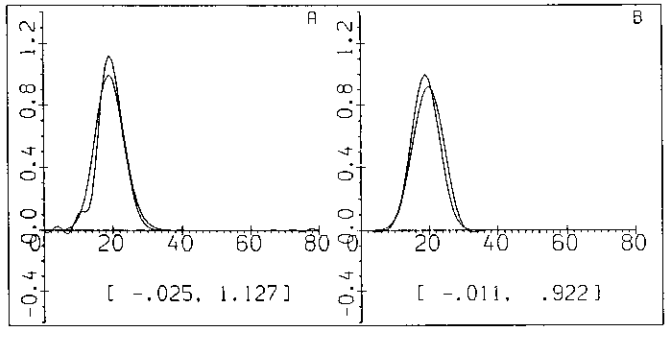

FIG. 3. 1D advection with $L_5^{(2)}$, CFL = 0.875: A—time stepping (9), B—time stepping (10).

where

$$u = u_0(\cos \varphi \cos \alpha + \sin \varphi \cos \lambda \sin \alpha),$$

$$v = u_0 \sin \lambda \sin \alpha,$$

$$q(\lambda, \varphi)|_{t=0} = \begin{cases} 500(1 + \cos(\pi r/R)) & \text{if } r < R \\ 0 & \text{if } r \geq R, \end{cases}$$

where a is the Earth radius, λ is longitude, φ is latitude, u is the λ-component of velocity, and v is its φ-component. The radius $R = a/3$ and the wind velocity $u_0 = 2\pi a/(12 \text{ days})$, r is the great circle distance between (λ, φ) and the center, initially taken as $(\lambda_c, \varphi_c) = (3\pi/2, 0)$:

$$r = a \arccos[\cos \varphi \cos(\lambda - 3\pi/2)].$$

The initial distribution of q is the cosine bell. It is shown by dashed lines in Fig. 4. The parameter α is the angle between the axis of solid body rotation and the polar axis of the spherical coordinate system. The flow over the poles corresponds to $\alpha = \pi/2$. The results for $\alpha = 0$ corresponding to the flow along the equator are of the same quality as for 1D tests with Gaussian initial distribution and are not shown.

The grid contained 128 points in longitude and 64 points in latitude. These grid parameters are the same as in [14] and some other papers. In this test flux correction was not used. Near the poles longitudinal Fourier filtering

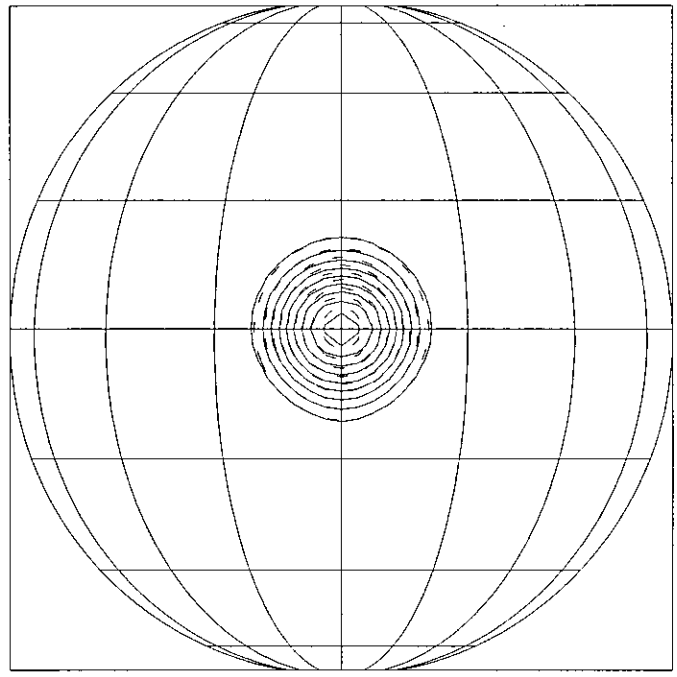

FIG. 4. 2D advection on the sphere with the flow over the poles for $L_5^{(2)}$ and time stepping (9), CFL = 0.2. The initial distribution is plotted by dashed lines. Plotting conventions are the same as in [12].

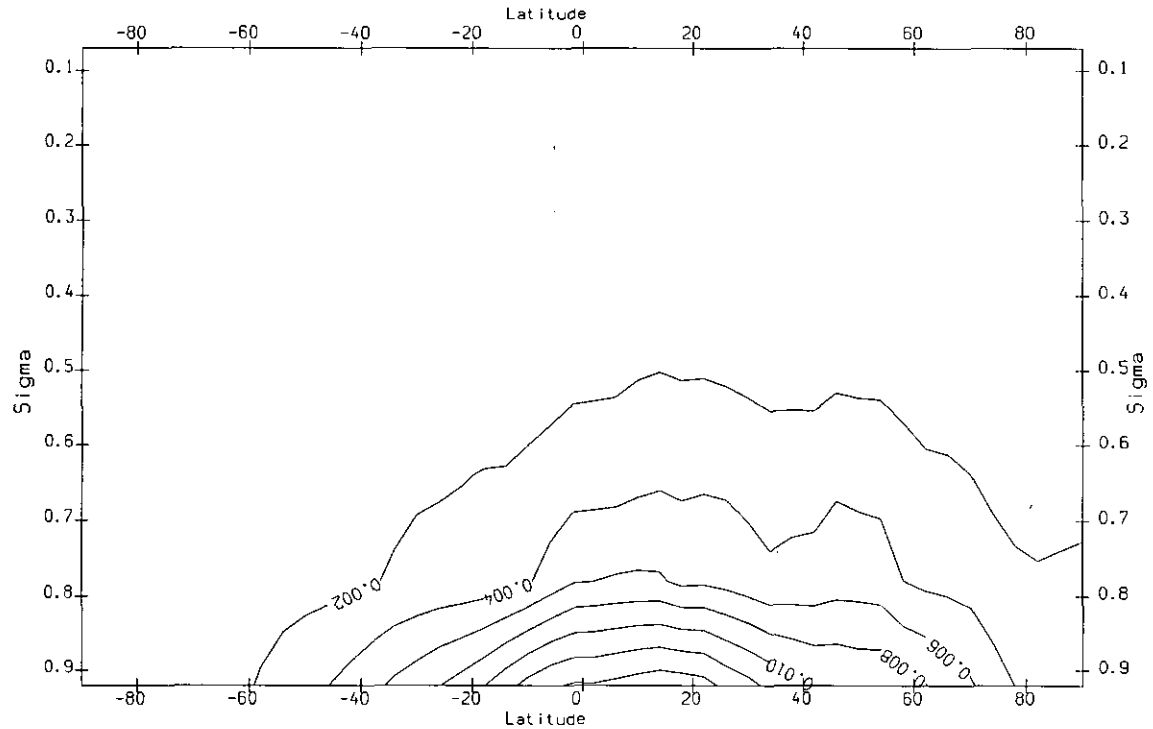

FIG. 8. The time-average zonal mean humidity for the first experiment (second-order horizontal discretization, explicit time scheme).

port algorithm in GCMA of INM. The moisture transport equation in GCMA is given as

$$\frac{\partial p_s q}{\partial t}+\frac{1}{a\cos\varphi}\left(\frac{\partial p_s u q}{\partial \lambda}+\frac{\partial p_s v\cos\varphi q}{\partial \varphi}\right)+\frac{\partial p_s \dot{\sigma} q}{\partial \sigma}=F, \qquad (11)$$

where $\sigma = p/p_s$ is the vertical coordinate (p_s is the sea-level pressure), F describes sinks and sources of moisture due to condensation and evaporation.

For approximation of space derivatives in horizontal directions CUD-5 discretization $L_5^{(2)}$ is used. Vertical

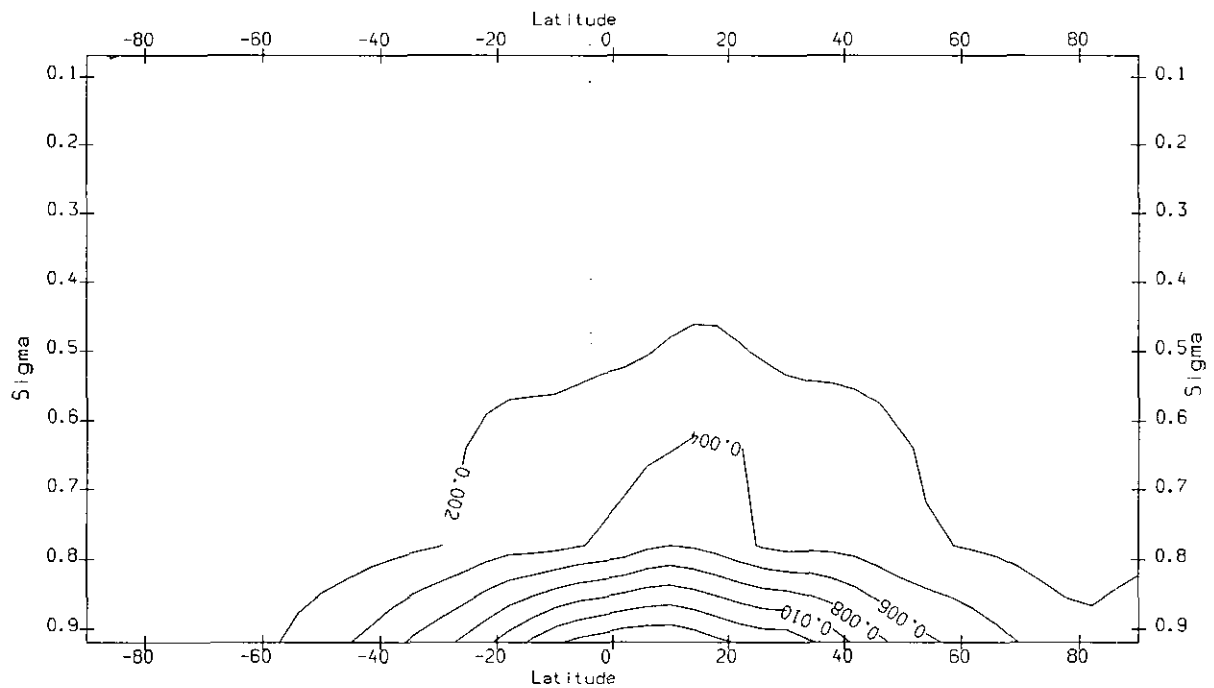

FIG. 9. The time-average zonal mean humidity for the second experiment (CUD-5 horizontal discretization, implicit time scheme).

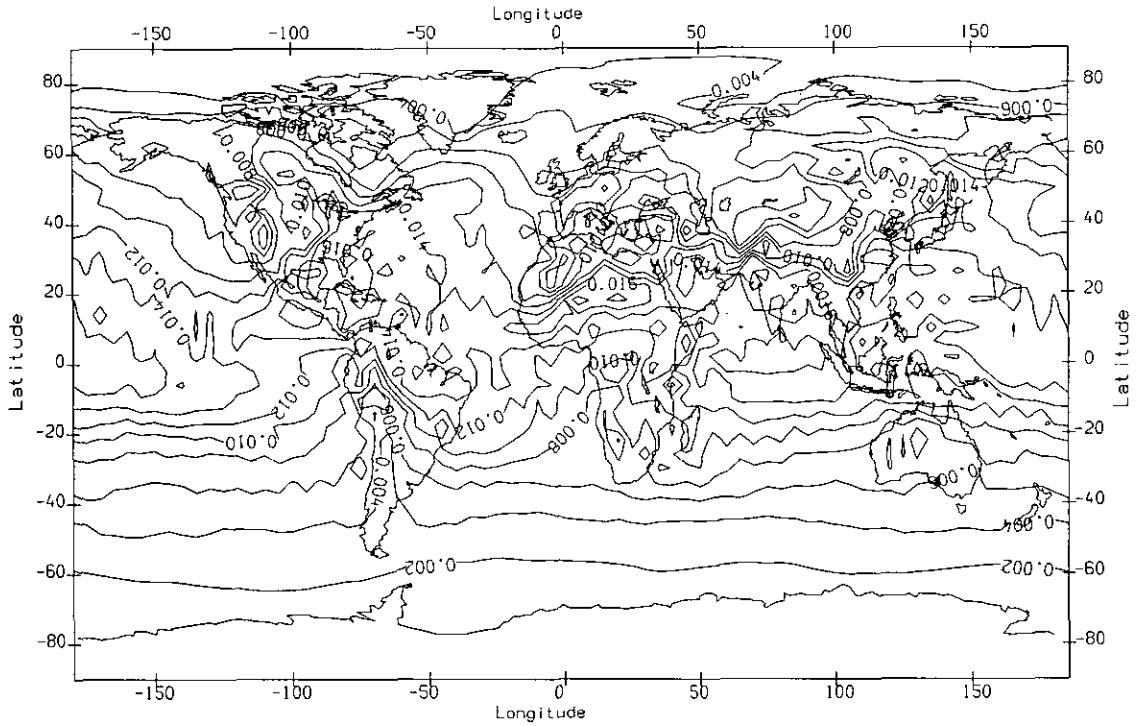

FIG. 10. The time-average humidity field at $\sigma = 0.92$ for the first experiment (second-order spatial discretization, explicit time scheme).

discretization is routine second-order central differencing on the staggered grid.

The implicit time stepping via the third-order conditionally stable scheme (9) was implemented with the help of the GMRES solver with Hausholder transformations [11]. Simple scaling of the matrix and the idea described in the previous section were used for faster convergence of iterations. It takes no more than eight iterations (two of them with the simple operator $\Lambda(s)$) for convergence with the relative accuracy 10^{-4}.

Two experiments were carried out. The first one was with the old version of moisture transport (i.e., with second-

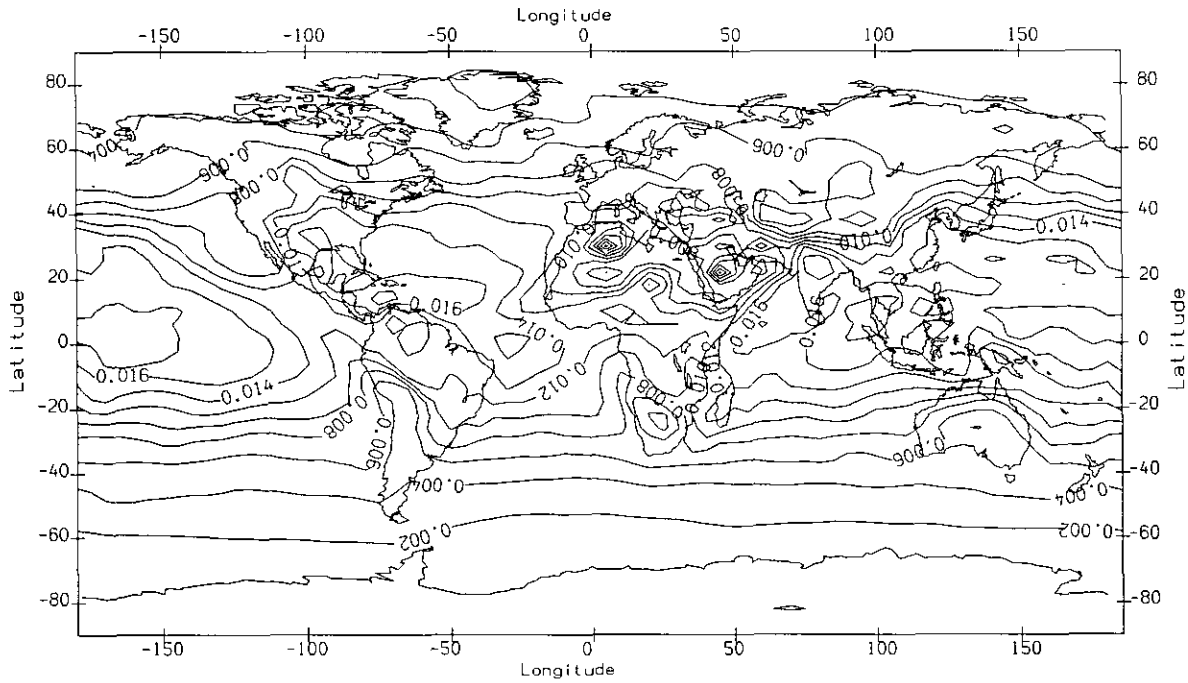

FIG. 11. The time-average humidity field at $\sigma = 0.92$ for the second experiment (CUD-5, implicit time scheme).

order central differencing and explicit time stepping), $\Delta t = 6$ min. The second experiment was with $L_5^{(2)}$ and the third-order implicit time stepping (9), $\Delta t = 60$ min. Initial conditions for GCMA were 1.06.1987 real data. The GCMA was integrated for 95 days. Here we describe only the results for the moisture. Time-averaged zonal mean (i.e., averaged over longitude) humidity field for the first (control) experiment is presented in Fig. 8, while Fig. 9 shows this field for the fifth-order experiment. We may see that for the second experiment the humidity field is much closer to the observed field. The false extremum in mid-latitudes vanished; the whole picture is more smooth. However, upon inspecting Fig. 9 we see a rather steep gradient near 20°. This gradient is explained by a rather coarse vertical mesh (seven equally spaced σ-levels) and central differencing by σ-coordinate. The analysis of vertical profiles of moisture confirms this observation. Thus an improvement in the vertical transport of moisture is also needed for the current version of the model. Comparing the geographical time-averaged distribution of humidity at the level $\sigma = 0.92$ for the control and fifth-order experiments (Figs. 10 and 11, respectively), we may see that the whole picture looks much better in the case of CUD-5. Hence, we may conclude that fifth-order compact upwind differencing is appropriate when solving a moisture transport equation.

Let us discuss now the cost of this scheme. The new scheme of moisture transport implemented via GMRES increases the computer time per one model day by 20%. However, the new version of our atmospheric model which is based on semi-implicit time stepping is 2.5 times faster and the cost of the new moisture transport becomes too expensive. So currently we are testing Runge–Kutta time stepping for moisture transport in the model. First experiments showed that the increase of time per model day is 20% for the new model.

3. DISCUSSION

The fifth-order compact upwind differencing used in this paper possesses the following favorable properties:

(i) small phase and amplitude errors,

(ii) conservation property,

(iii) compact stencil of approximation.

These properties were verified with several 1D and 2D tests. The implementation of this method for moisture transport in the general circulation model of the atmosphere has shown that it works much better than the previously used second-order explicit scheme. However, this method is rather costly. To increase its computational efficiency for unsteady problems time stepping should allow computations with a CFL number about one without significant errors due to time stepping. Further investigation of different time integration schemes is needed, especially the investigation of explicit Runge–Kutta schemes suitable for 3D problems.

APPENDIX

To study dispersion and dissipation properties of $L_5^{(1)}$ and $L_5^{(2)}$ operators we consider the wave solution of the 1D equation,

$$\frac{\partial u}{\partial t} + c\frac{\partial u}{\partial x} = 0. \tag{12}$$

To exclude the influence of time stepping, we write its semi-discretized form at the grid point $x = x_m$,

$$\begin{aligned} &\frac{du_m}{dt} + cL_5^{(n)}u_m = 0, \qquad n = 1, 2, \\ &\{x\} = x_m, \qquad m = 0, \pm 1, \ldots. \end{aligned} \tag{13}$$

Looking for the solution of (13) as $u_0 = U(t)\exp^{ixm}$, where $\alpha = kh$ is in the range of $[0, \pi]$, we obtain an ordinary differential equation of the form

$$\frac{dU}{dt} + cW(\alpha)\,U = 0, \tag{14}$$

where $W(\alpha)$ is Fourier image of $L_5^{(n)}$ which can be found easily to be

$$W(\alpha) = i\sin\alpha + 2s\sin^2\frac{\alpha}{2} - 2s \times \frac{(1 + 2\delta i\sin\alpha - 4\varepsilon\sin^2(\alpha/2))\sin^2(\alpha/2)}{(1 + 2\beta i\sin\alpha - 4\gamma\sin^2(\alpha/2))(1 - (1/3)\sin^2(\alpha/2))}.$$

The parameters are

$$\beta = \frac{1}{6s}, \qquad \gamma = 0.2, \qquad \delta = 0, \qquad \varepsilon = \frac{17}{60} - \frac{1}{9s^2}$$

for $L_5^{(1)}$ and

$$\beta = \frac{1}{10s} - 0.25s_1, \qquad \gamma = \frac{1}{6} - \frac{s_1}{10s},$$

$$\delta = -\frac{1}{15s} - 0.25s_1, \qquad \varepsilon = \frac{1}{6} + \frac{s_1}{15s}$$

in the case of $L_5^{(2)}$.

Comparing (14) with the equation $U' + ickU = 0$ obtained after substitution of $U(t)\exp^{ikx}$ in (12), we

obtain the ratio of the "scheme" phase velocity to the exact velocity c,

$$\frac{c^*}{c}=\frac{\Im mW(\alpha)}{\alpha}, \qquad \alpha=kh.$$

The dissipation property of $L_5^{(i)}$ is characterized by $\Re eW(\alpha)$. The graphs of dispersion and dissipation properties of $L_5^{(1)}$ and $L_5^{(2)}$ are shown in Figs. 12 and 13, respectively. In these graphs longer dashes correspond to greater values of s (or s_1, respectively). One can see that when increasing s (for $L_5^{(2)}$) or s_1 (for $L_5^{(2)}$) the dissipation increases. As far as dispersion is concerned, the minimal dispersion is obtained for $s=1.3$ in the case of $L_5^{(1)}$ and $s_1\approx 1.1$ in the case of $L_5^{(2)}$.

To study the stability limit for the time stepping procedure (9) we introduce time differencing into Eq. (14). Looking for the solution of this equation as

$$U_m^n=\lambda^n \exp^{imx},$$

we write the characteristic equation for time stepping (9)

$$\lambda-1+\left(\frac{5}{12}\lambda+\frac{8}{12}-\frac{1}{12}\frac{1}{\lambda}\right)rW(\alpha)=0,$$

where r is the CFL number. Solving this equation numerically and demanding that $|\lambda|\leqslant 1$ for all $\alpha\in[0,2\pi]$ we obtain that $r_{\max}$ should not exceed 0.7 in all considered cases for minimal admissible values of s and s_1, respectively. When increasing s (or s_1), the stability limit slightly increases. However, the remarkable property of the time stepping (9) is that the amplifying factor $|\lambda|$ beyond the stability limit is sufficiently close to one, unlike many explicit schemes. It was found that the algorithm admits local CFL numbers of order 1.3 during several time steps without loss of stability (in this case the amplifying factor for some harmonics is $|\lambda|\approx 1.05$).

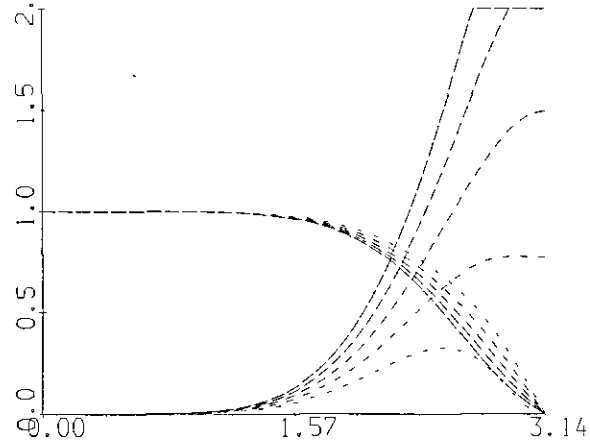

FIG. 12. The ratio of "scheme" phase velocity to the exact one and the relative dissipation of $L_5^{(1)}$ for various s as functions of grid wavenumber kh. Minimum value of s is 1.3, increment is 0.1. The longer dashes correspond to larger values of s.

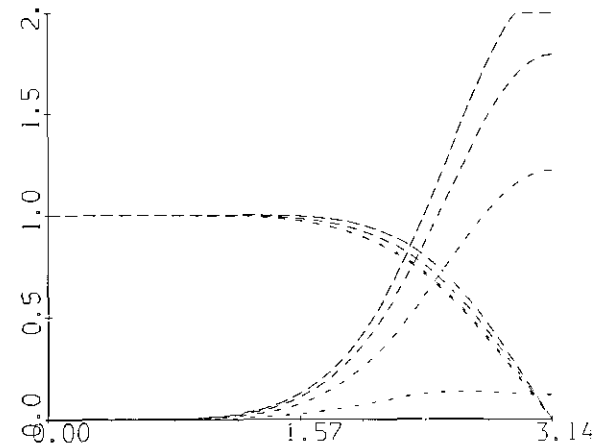

FIG. 13. The ratio of "scheme" phase velocity to the exact one and the relative dissipation of $L_5^{(2)}$ for various s_1 as functions of grid wavenumber kh. Minimum value of s_1 is 0.21, increment is 0.45. The longer dashes correspond to larger values of s_1.

ACKNOWLEDGMENTS

The author thanks his father, Professor A. I. Tolstykh, for helpful discussions. The idea of this work was strongly stimulated by his research. I also thank the anonymous referees whose comments helped to significantly improve the paper.

REFERENCES

1. P. J. Rasch and D. L. Williamson, *Quart. J. R. Meteorol. Soc.* **116**, 1071 (1990).
2. P. Smolarkiewicz and W. W. Grabowski, *J. Comput. Phys.* **86**, 355 (1990).
3. R. L. Carpenter, K. K. Droegemeier, P. R. Woodward, and C. E. Hane, *Mon. Weather Rev.* **118**, 586 (1990).
4. A. I. Tolstykh, *Sov. Math. Dokl.* **44**, 69 (1992).
5. G. A. Baker, Jr. and P. Graves-Morris, *Padé approximants*, Parts I, II (Addison-Wesley, Reading, MA, 1981).
6. A. I. Tolstykh, *High Accuracy Non-centered Compact Difference Scheme for Fluid Dynamics Applications* (World Scientific, Singapore, 1994).
7. M. A. Tolstykh, "High-Order Finite-Difference Techniques in Space and Time for Moisture Transport Equation in GCMA," in *Numerical Processes and Systems*, Vol. 10 (Nauka, Moscow, 1994). [Russian]
8. J. L. Steger and R. F. Warming, *J. Comput. Phys.* **40**, 263 (1981).
9. B. van Leer, *Lecture Notes in Phys.*, Vol. 170 (Springer-Verlag, New York/Berlin, 1982), p. 507.
10. A. I. Tolstykh, *Compact Difference Schemes and Their Application to Fluid Dynamics Problems* (Nauka, Moscow, 1990). [Russian]
11. H. F. Walker, *SIAM J. Sci. Stat. Comput.* **9**, 152 (1988).
12. D. L. Williamson, J. B. Drake, J. J. Hack, R. Jakob, and P. N. Swarztrauber, A standard test set for numerical approximations to the shallow water equations in spherical geometry, *J. Comput. Phys.* **102**, 211 (1992).
13. S. T. Zalesak, Fully multidimensional flux-corrected transport algorithms for fluids, *J. Comput. Phys.* **31**, 335 (1979).
14. P. K. Smolarkiewicz and P. J. Rasch, *J. Atmos. Sci.* **48**, 793 (1991).
15. L. L. Takacs and R. Balgovind, *Mon. Weather Rev.* **111**, 2005 (1983).
16. D. L. Williamson and P. J. Rasch, *Mon. Weather Rev.* **117**, 102 (1989).